Clim Dyn
DOI 10.1007/s00382-010-0939-3

Assessment of global dimming and brightening in IPCC-AR4/CMIP3 models and ERA40

Martin Wild · Edgar Schmucki

Received: 28 July 2010 / Accepted: 22 October 2010

Abstract Observations indicate that solar radiation incident at the Earth surface underwent substantial decadal variations in the second half of the twentieth century, with a tendency towards reduction from the 1950s to the 1980s ("global dimming") and a partial recovery thereafter ("brightening") at widespread locations. The most reliable observational records from the Global Energy Balance Archive (GEBA) are used to evaluate the ability of the climate models participating in CMIP3/IPCC-AR4 as well as the ERA40 reanalysis to reproduce these decadal variations. The results from 23 models and reanalysis are analyzed in five different climatic regions where strong decadal variations in surface solar radiation (SSR) have been observed. Only about half of the models are capable of reproducing the observed decadal variations in a qualitative way, and all models show much smaller amplitudes in these variations than seen in the observations. Largely differing tendencies between the models are not only found under all-sky conditions, but also in cloud-free conditions and in the representation of cloud effects. The ERA40 reanalysis neither reproduces the major decadal variations in SSR, despite strong observational constraints on the temporal evolution of the state of the atmosphere, since time varying aerosol loadings are missing. Climate models and reanalyses are therefore not yet at a stage to provide regionally consistent estimates of decadal changes in SSR. Reproduction of these changes would be essential for an adequate representation of regional scale climate variations and impacts, and short-term (decadal) climate projections.

M. Wild (✉) · E. Schmucki
Institute for Atmospheric and Climate Science, ETH Zurich, Universitätsstr. 16, 8092 Zurich, Switzerland
e-mail: martin.wild@env.ethz.ch

Keywords Climate change · Global climate modeling · Solar radiation · Climate variability · General circulation models

1 Introduction

An increasing number of studies suggests that solar radiation incident at the Earth surface (surface solar radiation, hereafter referred as SSR) is not stable over time but undergoes substantial decadal variations (Wild 2009a and references therein). Specifically, at many worldwide distributed sites a decrease in SSR has been noted between the 1950s and 1980s, popularly known as "global dimming" (Stanhill and Cohen 2001; Liepert 2002). A partial recovery was found more recently at a majority of the stations ("brightening", Wild et al. 2005). The substantial decadal changes in SSR are thought to have major impacts on various aspects of the climate system, such as global warming, the intensity of the hydrological cycle, glacier and snow cover changes, and terrestrial carbon uptake (see Wild 2009a for an overview). It is therefore important that global climate models (GCMs), major tools in climate research, are able to reproduce these variations in SSR.

In the present study we assess the ability of the GCMs used in the IPCC 4th assessment report (IPCC 2007) to reproduce the decadal variations of SSR over the second half of the twentieth century, using direct surface observations. These models are also known as CMIP3 models (3rd phase of the Coupled Model Intercomparison Project). A subset of these models has been compared with satellite-derived products of SSR for the period 1984–2000 in Romanou et al. (2007). In a recent study we pointed out that the decadal variations in surface warming as well as in the diurnal temperature range (DTR) are underestimated in

Published online: 16 November 2010

the IPCC-AR4/CMIP3 models (Wild 2009b). Since DTR variations were shown to be a useful indicator for SSR variations (e.g., Liu et al. 2004; Makowski et al. 2009), we argued that the lack of decadal variations in the simulated DTR may signify a lack of decadal variations in SSR in these models (Wild 2009b). Here we substantiate this argument further by assessing the SSR simulated in these models directly using ground based radiation observations.

2 Models and observational data

Simulations from the GCMs participating in the experiments for IPCC-AR4 (IPCC 2007) are used in the present analysis. These data have been organized by the Program for Climate Model Diagnosis and Intercomparison (PCMDI). We focus on the "Twentieth Century Climate in Coupled Models (20C3M)" experiments therein. These experiments were aimed at reproducing the climate evolution of the twentieth century as accurately as possible, by considering all major natural and anthropogenic forcings, such as changes in atmospheric greenhouse gases, aerosol load (tropospheric and volcanic), solar output, and land use. These experiments are therefore best suited for the assessment of the ability of the models to reproduce the climate evolution over the past decades. A more detailed description of the forcings used in these experiments is provided on the web pages of the PCMDI (http://www-pcmdi.llnl.gov/). In total, 23 models have been analyzed in this study. They are listed in Table 1, together with their home institution and their horizontal and vertical model resolution. Further given in Table 1 are the forcings related to aerosol direct and indirect effects, which can modify the simulated SSR, and which are most relevant for the present study. All models taking part in the IPCC-AR4/CMIP3 experiments consider to some extent changes in sulfate aerosol burden, but only three models include an explicit treatment of the sulfur cycle. Black carbon aerosols are only considered by a minority of the models (Table 1, last column). This applies also to the indirect aerosol effects (aerosol induced changes in cloud optical properties as well as cloud lifetime), which are not implemented in the majority of the models (Table 1, see also IPCC 2007, Table 10.1 for details of the individual models). Specifically, from the 23 models considered, 8 models include black and organic carbon, 7 models include the 1st indirect effect and 5 models include the 2nd indirect effect. Only three models include all these forcing agents, namely the MIROC3.2(hires), MIROC3.2(medres) and the UKMO-HadGEM1 models. From all models, simulated fluxes are analyzed for the period covering 1950–2000. This is the period where SSR variations are best known from the observational side, and which covers the characteristic "dimming" and "brightening" phases (see Wild (2009a) for an overview). Clear-sky fluxes are stored for 19 of the 23 models. No information on clear-sky fluxes is available from the models CSIRO-MK3.0, GISS-AOM, BCCR-BCM2.0, and PCM.

SSR fluxes as estimated in the reanalysis from the European Centre for Medium-Range Weather Forecasts (ECMWF) covering the period 1958–2002 (ERA-40, Uppala et al. 2005) are also used in this study. This extended integration period allows the assessment of both dimming and brightening phases. The atmospheric state of ERA-40 is constrained every 6 h by the assimilation of worldwide observations from the Global Observing System (GOS). However, ERA-40 does not include time varying tropospheric aerosols, but only a prescribed mean climatology (Tanre et al. 1984).

The observational reference data are taken from the Global Energy Balance Archive (GEBA), which has been established at ETH Zurich (Ohmura et al. 1989). Widespread measurements of SSR began in the 1950s. A hierarchy of quality control procedures has been applied to the GEBA data and erroneous energy fluxes are flagged (Gilgen and Ohmura 1999). The relative random error of a measurement is about 5% of a monthly mean and approximately 2% of a yearly mean (Gilgen et al. 1998). The dataset has been previously used for various applications, such as for the validation of model climatologies and satellite-derived products (e.g., Wild 2005), for the re-evaluation of the energy balance at the Earth's surface (Ohmura and Gilgen 1993), and the investigation of decadal variations in the observational records (e.g., Gilgen et al. 1998; Gilgen et al. 2009; Wild et al. 2005; Wild 2009a; Wild et al. 2009; Ohmura 2009).

For the present study, we selected some of the most reliable and extended records from GEBA for different regions of the world, as identified in Ohmura (2009). For the present analysis we defined five regions that have good data coverage and further depict characteristic decadal SSR variations: Europe, Japan, Southeast China, Northwest China and India. The stations used in the different regions along with their coordinates and period of measurements are given in Table 2 and correspond to those used in Ohmura (2009).

3 Methods

For the comparison of the model-calculated with the observed fluxes, the gridded monthly flux fields from the simulations were interpolated to the station coordinates given in Table 2, using a bilinear interpolation procedure, with distances computed along great circles on the sphere.

Table 1 Models participating in IPCC-AR4/CMIP3 and used in this study, with their affiliation, horizontal resolution and radiative forcing agents (black and organic carbon/1st indirect effect/2nd indirect effect)

Model ID	Institution, Country	Resolution (atmosphere)	Aeorosols: black and organic carbon/1st indirect/ 2nd indirect
CGCM3.1(T47)	Canadian Centre for Climate Modelling and Analysis, Canada	T47 (~2.8° × 2.8°), L31	N/N/N
CGCM3.1(T63)		T63 (~1.9° × 1.9°), L31	N/N/N
CSIRO-MK3.0	Commonwealth Scientific and Industrial Research Organisation (CSIRO) Atmospheric Research, Australia	T63 (~1.9° × 1.9°), L18	N/N/N
CSIRO-MK3.5		T63 (~1.9° × 1.9°), L18	N/N/N
GFDL-CM2.0	U.S. Department of Commerce/National Oceanic and Atmospheric Administration (NOAA)/ Geophysical Fluid Dynamics Laboratory (GFDL), USA	2.0° × 2.5°, L24	Y/N/N
GFDL-CM2.1		2.0° × 2.5°, L24	Y/N/N
MIROC3.2(hires)	Center for Climate System Research (University of Tokyo), National Institute for Environmental Studies and Frontier Research Center for Global Change (JAMSTEC), Japan	T106 (~1.1° × 1.1°), L56	Y/Y/Y
MIROC3.2(medres)		T42 (~2.8° × 2.8°), L20	Y/Y/Y
INM-CM3.0	Institute for Numerical Mathematics, Russia	4° × 5°, L21	N/N/N
IPSL-CM4	Institut Pierre Simon Laplace, France	2.5° × 3.75°, L19	N/Y/N
ECHAM5/MPI-OM	Max Planck Institute for Meteorology, Germany	T63 (~1.9° × 1.9°), L31	N/Y/N
ECHO-G	Meteorological Institute of the University of Bonn, Meteorological Research Institute of the Korea Meteorological Administration (KMA), and Model and Data Group, Germany/Korea	T30 (~3.9° × 3.9°), L19	N/Y/N
GISS-AOM	National Aeronautics and Space Administration (NASA)/Goddard Institute for Space Studies (GISS), USA	3° × 4°, L12	N/N/N
GISS-ER		4° × 5°, L20	Y/N/Y
MRI-CGCM2.3.2	Meteorological Research Institute, Japan	T42 (~2.8° × 2.8°), L30	N/N/N
CNRM-CM3	Météo-France/Centre National de Recherches Météorologiques, France	T63 (~1.9° × 1.9°), L45	N/N/N
FGOALS-g1.0	National Key Laboratory of Numerical Modeling for Atmospheric Sciences and Geophysical Fluid Dynamics (LASG)/Institute of Atmospheric Physics, China	T42 (~2.8° × 2.8°), L26	N/N/N
GISS-EH	NASA/GISS, USA	4° × 5°, L20	Y/N/Y
BCCR-BCM2.0	Bjerknes Centre for Climate Research, Norway	T63 (~1.9° × 1.9°), L31	N/N/N
CCSM3	National Center for Atmospheric Research, USA	T85 (~1.4° × 1.4°), L26	Y/N/N
PCM	National Center for Atmospheric Research, USA	T42 (~2.8° × 2.8°), L26	N/N/N
UKMO-HadCM3	Hadley Centre for Climate Prediction and Research/Met Office, UK	2.5° × 3.75°, L19	N/Y/N
UKMO-HadGEM1		~1.3° × 1.9°, L38	Y/Y/Y

Y forcing agent included, *N* not included

Tests have shown that the trends at the grid points surrounding a station do not differ significantly from each other in most of the cases, so that the choice of the interpolation scheme is not critical.

Collocated observed and simulated monthly time series were thereby obtained at each station and were further aggregated into annual mean time series. Annual anomalies were determined as deviations from their long term mean for each time series. The individual annual anomaly time series were then averaged within the five world regions to obtain simulated and observed composite time series for each of the respective regions mentioned above. The averaging over anomalies rather than over absolute values avoids the introduction of spurious trends in the composite time series due to potential data gaps at individual observation sites.

The time series were then fitted with first or second order polynomials of the form $f(x) = bx + c$, and $f(x) = ax^2 + bx + c$, respectively, depending on the overall shape of the observed composite time series.

Table 2 GEBA stations with long term observational SSR records in the five world regions used in this study

Region	Station name (country)	Latitude [°N]	Longitude [°E]	Period of measurements
Europe	Stockholm (Sweden)	59.4	18.0	1922–2006
	Wageningen (Netherlands)	52.0	5.7	1928–2000
	Potsdam (Germany)	52.4	13.1	1937–1998
	Locarno-Monti (Switzerland)	46.2	8.8	1938–2005
	Hamburg (Germany)	53.7	10.1	1949–2006
	Hohenpeissenberg (Germany)	47.8	11.0	1953–1998
	Sodankyla (Finland)	67.4	26.7	1953–2006
	Taastrup/Copenhagen (Denmark)	55.7	12.3	1965–2002
	Toravere (Estonia)	58.5	26.8	1955–1994
Japan	Sapporo	43.1	141.3	1957–2006
	Morioka	39.7	141.2	1961–2002
	Akita	39.7	140.1	1961–2006
	Sendai	38.3	140.9	1957–2002
	Fukushima	37.8	140.5	1961–2002
	Yamagata	38.3	140.4	1961–2002
	Onahama	37.0	140.9	1961–2002
	Takada	37.1	138.3	1961–2002
	Tateno	36.1	140.1	1957–2002
	Tokyo	35.7	139.8	1961–2002
	Nagoya	35.0	137.0	1961–2002
	Hikone	35.3	136.3	1961–2002
	Yonago	35.4	133.4	1961–2006
	Maizuru	35.5	135.3	1961–2002
	Shimonoseki	34.0	130.9	1961–2002
	Hiroshima	34.4	132.5	1961–2002
	Nara	34.7	135.8	1961–2002
	Izuhara	34.2	129.3	1961–2002
	Saga	33.3	130.3	1961–2002
	Kumamoto	32.8	130.7	1961–2002
	Matsuyama	33.9	132.8	1961–2002
	Takamatsu	34.3	134.1	1961–2002
	Kochi	33.6	133.6	1961–2002
	Shimizu/Ashizuri	32.7	133.0	1961–2006
	Naha	26.2	127.7	1961–2006
Southeast China	Fuzhou	26.1	119.3	1961–2000
	Ganzhou	25.9	115.0	1961–2000
	Haikou	20.0	110.4	1961–2000
	King's Park (Hong Kong)	22.3	114.2	1984–2002
	Shanghai (1961–1990)	31.2	121.4	1961–1990
	Shantou	23.4	116.7	1961–2000
Northwest China	Altay	47.7	88.1	1960–2000
	Hami	42.8	93.5	1961–2000
	Kuqa	41.8	82.9	1957–1990
	Turpan	42.9	89.2	1960–2000
	Urumqi	43.8	87.6	1959–2005
	Yining	44.0	81.3	1960–2000
	Lanzhou	36.1	103.9	1959–2003
India	Ahmadabad	23.1	72.6	1964–2005
	Trivandrum	8.5	77.0	1964–2005
	Nagpur/Sonegaon	21.1	79.1	1964–2005
	Vishakhapatnam	17.7	83.2	1964–2005

4 Results

Simulated and observed decadal SSR changes in the different regions are discussed in the following subsections. The climatological mean SSR fields in these models have been evaluated in earlier studies for both clear-sky (Wild et al. 2006) and all-sky conditions (Wild 2008).

4.1 Europe

Various studies presented evidence that SSR over Europe has undergone significant changes over the past decades, with a predominant decline measured at many sites between the 1950s and 1980s, and partial recovery thereafter (e.g., Ohmura and Lang 1989; Stanhill and Cohen 2001; Wild et al. 2005; Norris and Wild 2007; Chiacchio and Wild 2010).

This tendency can also be seen in the observed composite time series based on annual anomalies at nine sites selected in this study in Fig. 1 (upper panel). A substantial decline of surface solar radiation on the order of 10 Wm^{-2} can be seen until the mid 1980s in the observations, followed by an increase after the late 1980s of a few Wm^{-2}. In addition shown are the model-simulated composite time series averaged over the same locations, representing all-sky SSR as in the observations. All composite time series were constructed as outlined in Sect. 3 and have been smoothed with a 5-year running mean.

The qualitative tendency with a decrease in the first part of the record, and some sign of recovery in the latter part, can be best represented by a second order polynomial model. This is applied to both model-simulated and observed time series in Fig. 1. We use the term "convex" in the following to qualitatively describe the evolution of the time series with a decrease and subsequent increase (or alternatively stated a positive coefficient in the quadratic term of the second order polynomial model, with a turning point at the local minimum). Similarly, the term "concave" is used here to describe the evolution of the time series with an initial increase and a subsequent decrease (or alternatively stated a negative coefficient in the quadratic term of the second order polynomial model, and a turning point at the local maximum). According to this definition, the observed time series shows a convex evolution (see Fig. 1, upper panel). It is obvious from Fig. 1 (upper panel) that the simulated all-sky SSR evolution at these European sites largely differs between the 23 models. Only about half of the models reproduce the convex shape of the overall evolution, indicative of a "dimming" followed by a "brightening", the other half of the models show a concave shape in their second order polynomial approximation, indicative of an opposite qualitative evolution compared to the observed tendencies. Specifically, Table 3 (first

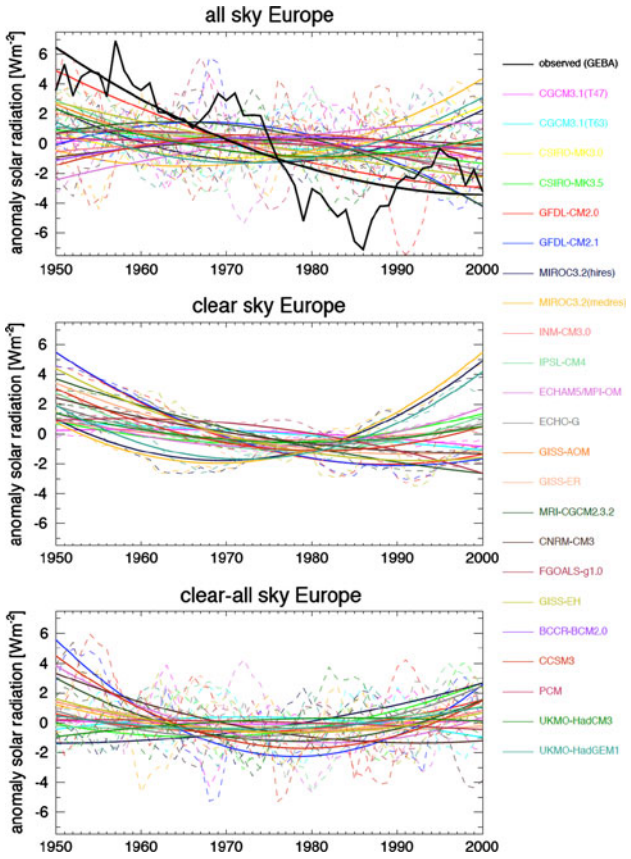

Fig. 1 Observed annual SSR anomalies from 1950 to 2000 as composite of nine sites in Europe (in *black*), and corresponding simulations by 23 climate models (in *color*, *dashed*). Reference period is 1950–2000. All-sky fluxes shown in upper panel, clear-sky fluxes in middle panel, surface cloud effect (defined as difference of clear- and all-sky fluxes) in lower panel. Observations are only available for all-sky conditions. Time series shown as 5-year running means. Also added are second order polynomial fits (*solid lines*)

column) shows that the quadratic ('a') coefficient of the observations in Europe is 0.0037 $Wm^{-2}a^{-2}$, and significant at the 66% level (in the following we use the default term "significant" for a statistical significance at the 66% level, if not otherwise mentioned). The quadratic coefficients in the models range from −0.0053 (GFDL-CM2.1) to 0.0057 $Wm^{-2}a^{-2}$ (MIROC3.2(hires)), with 11 models having a negative coefficient and 12 models having a positive one. Of the 11 models that show a concave behavior in their time series, 4 are significant, while of the 12 models showing a convex behavior 7 are significant.

For further comparison we separate the time series into two periods with distinctly different tendencies in the observations, one representing the "dimming" period 1960–1985, the second one the "brightening" period 1985–2000, and allow for linear approximations during these periods. The observed decrease of solar radiation from 1960 to 1985 at the European sites amounts to

Table 3 Second order polynomial fit coefficients ('a'-coefficient) for the SSR composite time series of the sites in Europe, Japan and southeast China, and linear fit coefficients ('b'-coefficient) for the SSR composite time series of sites in northwest China and India together with the 1-sigma uncertainty in italics as calculated from observations and corresponding IPCC-AR4/CMIP3 model simulations

Surface solar radiation	Europe		Japan		Southeast China		Northwest China		India	
	Polynomial trend 1950–2000 $\mathbf{a}x^2$	*1-sigma uncertainty*	Polynomial trend 1961–2000 $\mathbf{a}x^2$	*1-sigma uncertainty*	Polynomial trend 1961–2000 $\mathbf{a}x^2$	*1-sigma uncertainty*	Linear trend 1960–2000 **b**x	*1-sigma uncertainty*	Linear trend 1964–2000 **b**x	*1-sigma uncertainty*
GEBA	**0.0037**	*0.0031*	**0.0295**	*0.0059*	**0.0476**	*0.0085*	**−0.5146**	*0.0583*	**−0.6864**	*0.1088*
CGCM3.1(T47)	−0.0011	*0.0025*	**−0.0060**	*0.0034*	−0.0032	*0.0073*	**−0.0682**	*0.0307*	0.0233	*0.0660*
CGCM3.1(T63)	0.0013	*0.0022*	0.0024	*0.0047*	−0.0001	*0.0064*	−0.0295	*0.0355*	**−0.0799**	*0.0507*
CSIRO-MK3.0	**0.0040**	*0.0020*	−0.0023	*0.0041*	−0.0019	*0.0116*	−0.0060	*0.0231*	**−0.1109**	*0.0852*
CSIRO-MK3.5	−0.0005	*0.0023*	**−0.0074**	*0.0058*	−0.0099	*0.0116*	−0.0136	*0.0414*	−0.0304	*0.1124*
GFDL-CM2.0	0.0025	*0.0034*	−0.0035	*0.0073*	−0.0053	*0.0084*	**−0.1235**	*0.0395*	**−0.1589**	*0.0800*
GFDL-CM2.1	**−0.0053**	*0.0027*	0.0032	*0.0065*	0.0041	*0.0119*	**−0.0931**	*0.0396*	0.0193	*0.0960*
MIROC3.2(hires)	**0.0057**	*0.0022*	**0.0049**	*0.0041*	**−0.0096**	*0.0061*	**−0.0815**	*0.0268*	**−0.1714**	*0.0563*
MIROC3.2(medres)	**0.0048**	*0.0031*	**0.0069**	*0.0052*	0.0058	*0.0076*	**−0.1061**	*0.0287*	**−0.1727**	*0.0630*
INM-CM3.0	−0.0010	*0.0015*	−0.0020	*0.0049*	−0.0042	*0.0078*	−0.0137	*0.0344*	−0.1153	*0.1215*
IPSL-CM4	**0.0038**	*0.0026*	−0.0033	*0.0050*	0.0009	*0.0075*	−0.0409	*0.0422*	0.0177	*0.0610*
ECHAM5/MPI-OM	−0.0012	*0.0032*	−0.0009	*0.0078*	0.0013	*0.0112*	**−0.1583**	*0.0371*	−0.0264	*0.0909*
ECHO-G	−0.0008	*0.0029*	0.0008	*0.0055*	0.0053	*0.0098*	**−0.0631**	*0.0560*	**−0.1930**	*0.0458*
GISS-AOM	**0.0035**	*0.0019*	**−0.0066**	*0.0039*	−0.0006	*0.0044*	**−0.1108**	*0.0236*	**−0.0702**	*0.0282*
GISS-ER	0.0014	*0.0023*	**0.0068**	*0.0045*	**0.0130**	*0.0066*	**−0.2224**	*0.0457*	**−0.3997**	*0.0580*
MRI-CGCM2.3.2	**−0.0042**	*0.0021*	−0.0012	*0.0061*	−0.0070	*0.0079*	0.0335	*0.0390*	**−0.0751**	*0.0464*
CNRM-CM3	−0.0012	*0.0027*	0.0035	*0.0063*	**0.0190**	*0.0077*	−0.0222	*0.0326*	**−0.0977**	*0.0693*
FGOALS-g1.0	**−0.0018**	*0.0017*	**−0.0078**	*0.0042*	**−0.0177**	*0.0063*	−0.0133	*0.0213*	0.0454	*0.0706*
GISS-EH	0.0006	*0.0023*	**0.0195**	*0.0043*	0.0060	*0.0061*	**−0.1816**	*0.0604*	**−0.2835**	*0.0574*
BCCR-BCM2.0	**−0.0020**	*0.0018*	0.0061	*0.0066*	−0.0036	*0.0093*	−0.0151	*0.0245*	**−0.1035**	*0.0626*
CCSM3	−0.0030	*0.0040*	**−0.0063**	*0.0045*	0.0019	*0.0085*	−0.0147	*0.0439*	**−0.2280**	*0.0740*
PCM	0.0000	*0.0039*	−0.0056	*0.0068*	−0.0046	*0.0083*	−0.0275	*0.0373*	**−0.1351**	*0.0972*
UKMO-HadCM3	**0.0034**	*0.0022*	0.0010	*0.0047*	0.0072	*0.0081*	−0.0396	*0.0517*	**−0.1171**	*0.0745*
UKMO-HadGEM1	**0.0056**	*0.0023*	**−0.0111**	*0.0064*	0.0051	*0.0076*	−0.0312	*0.0327*	**−0.2055**	*0.0711*
Multimodel mean	0.0006		−0.0004		0.0001		−0.0627		−0.1160	
Multimodel median	0.0000		−0.0012		−0.0001		−0.0396		−0.1109	

Coefficients exceeding the 1-sigma uncertainty are highlighted in bold, values in italics are statistically significant at the 66% level. Units: $Wm^{-2}a^{-2}$ for the a-coefficient, $Wm^{-2}a^{-1}$ for the linear trend

Table 4 Linear trends of SSR composite time series of the sites in Europe, Japan, southeast China, northwest China and India for two time periods representing "dimming" and "brightening" together with their 1-sigma uncertainty in italics as calculated from observations and corresponding IPCC-AR4/CMIP3 model simulations

Surface solar radiation	Europe		Japan		Southeast China		Northwest China		India	
	Linear trend: 1960–1985 1985–2000	*1-sigma uncertainty*	Linear trend: 1961–1985 1985–2000	*1-sigma uncertainty*	Linear trend: 1961–1985 1985–2000	*1-sigma uncertainty*	Linear trend: 1960–1985 1985–2000	*1-sigma uncertainty*	Linear trend: 1964–1985 1985–2000	*1-sigma uncertainty*
GEBA	**−0.328**	*0.097*	**−0.553**	*0.126*	**−1.230**	*0.182*	**−0.649**	*0.113*	**−0.544**	*0.097*
	0.232	*0.204*	**0.577**	*0.287*	**0.682**	*0.294*	−0.208	*0.233*	**−1.969**	*0.344*
CGCM3.1(T47)	**0.113**	*0.101*	**0.133**	*0.057*	0.050	*0.164*	**−0.053**	*0.053*	−0.144	*0.143*
	0.212	*0.139*	0.099	*0.155*	−0.245	*0.267*	**0.174**	*0.136*	−0.074	*0.245*
CGCM3.1(T63)	0.005	*0.078*	0.078	*0.088*	−0.012	*0.120*	−0.061	*0.063*	0.072	*0.110*
	0.324	*0.150*	**0.366**	*0.200*	0.116	*0.312*	−0.130	*0.169*	**−0.385**	*0.177*
CSIRO-MK3.0	−0.070	*0.075*	−0.059	*0.085*	−0.135	*0.165*	−0.022	*0.049*	**−0.295**	*0.197*
	0.416	*0.144*	**−0.268**	*0.162*	−0.605	*0.617*	**0.140**	*0.081*	0.037	*0.271*
CSIRO-MK3.5	0.018	*0.083*	0.065	*0.123*	0.049	*0.280*	0.014	*0.081*	0.144	*0.263*
	−0.335	*0.175*	0.095	*0.243*	**−0.521**	*0.309*	0.165	*0.175*	−0.349	*0.351*
GFDL-CM2.0	**−0.183**	*0.091*	−0.052	*0.128*	**−0.240**	*0.152*	**−0.080**	*0.071*	−0.009	*0.186*
	−0.214	*0.347*	−0.258	*0.365*	**−0.744**	*0.379*	**−0.350**	*0.186*	−0.111	*0.264*
GFDL-CM2.1	**−0.114**	*0.107*	**−0.197**	*0.145*	**−0.427**	*0.249*	−0.055	*0.074*	0.057	*0.190*
	−0.142	*0.224*	−0.242	*0.246*	**−0.509**	*0.460*	−0.131	*0.181*	**−0.382**	*0.377*
MIROC3.2(hires)	−0.013	*0.081*	−0.074	*0.085*	**−0.212**	*0.125*	**−0.051**	*0.049*	**−0.295**	*0.147*
	0.193	*0.127*	0.097	*0.182*	**−0.872**	*0.222*	0.086	*0.119*	−0.025	*0.125*
MIROC3.2(medres)	−0.106	*0.122*	**−0.315**	*0.102*	**−0.410**	*0.160*	**−0.062**	*0.059*	**−0.327**	*0.122*
	0.377	*0.201*	0.108	*0.220*	−0.086	*0.314*	−0.102	*0.111*	0.169	*0.248*
INM-CM3.0	**0.067**	*0.046*	−0.099	*0.115*	0.019	*0.162*	**−0.116**	*0.070*	−0.132	*0.261*
	−0.071	*0.121*	**−0.250**	*0.148*	−0.047	*0.319*	**0.168**	*0.121*	0.077	*0.453*
IPSL-CM4	**0.173**	*0.080*	**0.121**	*0.109*	**−0.300**	*0.170*	**−0.080**	*0.080*	0.075	*0.132*
	−0.051	*0.218*	0.010	*0.190*	−0.137	*0.284*	**−0.291**	*0.173*	0.028	*0.231*
ECHAM5/MPI-OM	0.094	*0.113*	−0.148	*0.159*	−0.088	*0.250*	**−0.230**	*0.069*	−0.165	*0.222*
	−0.167	*0.220*	−0.119	*0.332*	0.010	*0.401*	**−0.200**	*0.165*	**0.300**	*0.251*
ECHO-G	0.055	*0.110*	**−0.099**	*0.073*	−0.177	*0.213*	−0.120	*0.124*	−0.031	*0.093*
	−0.254	*0.184*	0.063	*0.318*	**−0.447**	*0.383*	0.115	*0.177*	−0.391	*0.165*
GISS-AOM	0.033	*0.070*	−0.015	*0.076*	0.002	*0.078*	**−0.192**	*0.050*	0.001	*0.070*
	0.121	*0.136*	**−0.278**	*0.179*	**0.248**	*0.219*	−0.042	*0.090*	−0.009	*0.077*
GISS-ER	0.024	*0.092*	**−0.335**	*0.088*	**−0.395**	*0.128*	**−0.174**	*0.091*	**−0.124**	*0.115*
	−0.310	*0.161*	−0.054	*0.215*	0.255	*0.294*	−0.034	*0.210*	**−0.702**	*0.212*
MRI-CGCM2.3.2	**−0.111**	*0.086*	**−0.144**	*0.114*	0.118	*0.167*	0.053	*0.085*	−0.042	*0.100*
	0.039	*0.145*	**−0.551**	*0.275*	−0.002	*0.330*	0.012	*0.137*	−0.062	*0.172*

Table 4 continued

Surface solar radiation	Europe		Japan		Southeast China		Northwest China		India	
	Linear trend: 1960–1985 1985–2000	*1-sigma uncertainty*	Linear trend: 1961–1985 1985–2000	*1-sigma uncertainty*	Linear trend: 1961–1985 1985–2000	*1-sigma uncertainty*	Linear trend: 1960–1985 1985–2000	*1-sigma uncertainty*	Linear trend: 1964–1985 1985–2000	*1-sigma uncertainty*
CNRM-CM3	**−0.110**	*0.092*	**−0.303**	*0.141*	**−0.475**	*0.140*	−0.064	*0.072*	0.100	*0.141*
	0.426	*0.175*	0.001	*0.213*	**0.523**	*0.351*	0.092	*0.121*	**−0.318**	*0.258*
FGOALS-g1.0	−0.059	*0.068*	0.034	*0.091*	**0.182**	*0.141*	0.062	*0.042*	−0.065	*0.124*
	−0.293	*0.126*	**−0.302**	*0.171*	**−0.555**	*0.232*	**−0.109**	*0.094*	**0.379**	*0.295*
GISS-EH	−0.058	*0.071*	**−0.444**	*0.092*	**−0.342**	*0.131*	**−0.241**	*0.121*	**−0.190**	*0.126*
	−0.362	*0.174*	**0.347**	*0.170*	**−0.607**	*0.207*	−0.052	*0.249*	−0.010	*0.183*
BCCR-BCM2.0	**0.155**	*0.068*	−0.129	*0.140*	−0.011	*0.197*	−0.030	*0.050*	0.020	*0.155*
	−0.174	*0.128*	−0.042	*0.267*	−0.116	*0.361*	−0.030	*0.102*	−0.160	*0.179*
CCSM3	0.041	*0.142*	**0.125**	*0.081*	−0.064	*0.166*	**0.059**	*0.050*	−0.025	*0.124*
	−0.435	*0.319*	**−0.234**	*0.210*	**−0.481**	*0.400*	0.047	*0.198*	−0.131	*0.320*
PCM	−0.111	*0.167*	−0.097	*0.148*	**0.211**	*0.161*	**−0.094**	*0.070*	−0.070	*0.228*
	0.203	*0.200*	**−0.495**	*0.242*	0.127	*0.365*	−0.051	*0.173*	**−0.504**	*0.304*
UKMO-HadCM3	**−0.184**	*0.081*	**−0.140**	*0.089*	**−0.247**	*0.160*	**−0.186**	*0.096*	−0.120	*0.199*
	0.214	*0.121*	−0.094	*0.222*	0.172	*0.357*	0.001	*0.222*	0.107	*0.183*
UKMO-HadGEM1	0.072	*0.075*	**0.250**	*0.132*	−0.115	*0.150*	0.017	*0.072*	−0.164	*0.166*
	0.232	*0.156*	**−0.403**	*0.251*	0.256	*0.316*	**−0.246**	*0.108*	**−0.548**	*0.233*
Multimodel mean	−0.012		−0.080		−0.131		−0.074		−0.075	
	−0.002		−0.105		−0.186		−0.033		−0.133	
Multimodel median	0.005		−0.097		−0.115		−0.062		−0.065	
	−0.051		−0.094		−0.116		−0.034		−0.074	

Coefficients exceeding the 1-sigma uncertainty are highlighted in bold, values in italics are statistically significant at the 66% level. Units: $Wm^{-2}a^{-1}$

-0.328 $Wm^{-2}a^{-1}$ and is to 95% significant (Table 4). The linear trends in the models between 1960 and 1985 vary from -0.183 $Wm^{-2}a^{-1}$ in the GFDL-CM2.0 model to 0.173 $Wm^{-2}a^{-1}$ in the IPSL-CM4, with a multi-model mean slope -0.012 $Wm^{-2}a^{-1}$. None of the models thus captures the observed decrease quantitatively. 11 models show at least a decline of SSR during this period in qualitative agreement with the observations (5 of them significant), even though strongly underestimated. However, 12 models show an increase in this period (4 of them significant), in contrast to the observations. During the "brightening" period 1985–2000 the observed increase of SSR is 0.232 $Wm^{-2}a^{-1}$ and significant. The linear trends in the models vary in a range between -0.435 $Wm^{-2}a^{-1}$ (CCSM3) and 0.426 $Wm^{-2}a^{-1}$ (CNRM-CM3), with a multi-model mean slope of -0.002 $Wm^{-2}a^{-1}$. 11 models show an increase in SSR in qualitative agreement with the observations (9 of them significant), while 12 models show a decrease (7 of them significant) in contrast to the observational evidence.

This suggests that models largely differ in their simulation of decadal variations in SSR over Europe, and that many models are barely capable of reproducing the observed trends even qualitatively. The individual model deviations are further quantified in terms of the root mean squared error (RMS) of the simulated compared to the observed SSR composite time series (Table 5). The RMS statistics have been determined based on the 5-year running means of the time series, since climate models cannot expected to be deterministic on short interannual timescales, and deviations induced by these year-to-year variations are therefore meaningless.

Further shown in Fig. 1 are the model-simulated SSR annual anomalies time series averaged over the same sites under cloud-free conditions (middle panel), as well as the simulated cloud effect on SSR (lower panel). The cloud effect is defined here as difference between the SSR time series under clear-sky (middle panel) and all-sky (upper panel) conditions. These quantities are shown for those 19 out of the 23 models that provide clear-sky information (see Sect. 2). For these quantities we do not have direct observations for comparison, since only monthly mean observations are available of these long-term multidecadal records, which do not allow for a strict separation into clear- and cloudy-skies. Nevertheless it is interesting to explore the level of consistency in the model simulations under clear-sky conditions. Under these conditions, more models show an SSR time series of convex shape, in qualitative agreement with the (all-sky) observations. 16 out of the 19 models show such a behavior under clear-sky conditions, compared to 12 models out of 23 models under all-sky conditions. Correlations between both simulated clear-sky and all-sky time series and the (all-sky) observations are given in Table 6. All correlations are based on the time series smoothed with 5-year running means, to compare the lower frequency variations in models and observations rather than the interannual variations which are not deterministic in GCMs. Interestingly, correlations are typically higher when the (all-sky) observations are correlated with the simulated clear-sky fluxes than with the simulated all-sky fluxes (Table 6). This applies for 14 out of the 19 models that provide both all-sky and clear-sky fluxes. Specifically, when averaged over the 19 models, the correlation between the (all-sky) observations and the simulated clear-sky fluxes is 0.46 (maximum correlation 0.88, CNRM-CM3), but only 0.12 (maximum correlation 0.68, UKMO-HadCM3) between the (all-sky) observations and the more directly related simulated all-sky fluxes (Table 6). This suggests that the model-simulated decadal cloud variations rather deteriorate than improve the simulation of SSR. Thus the decadal variations in the cloud effect on SSR given in the lower

Table 5 Yearly root mean squared error (RMS) of the SSR composite time series at the sites in Europe, Japan, southeast China, northwest China and India as simulated by the 23 models participating in IPCC-AR4/CMIP3

RMS	Europe	Japan	China SE	China NW	India
CGCM3.1(T47)	3.83	3.74	5.76	6.13	11.57
CGCM3.1(T63)	3.61	3.31	5.05	5.92	11.47
CSIRO-MK3.0	3.68	3.39	5.65	6.52	10.63
CSIRO-MK3.5	3.51	3.50	5.63	6.52	11.90
GFDL-CM2.0	3.22	5.48	6.17	5.14	10.19
GFDL-CM2.1	3.28	3.48	6.19	5.99	11.06
MIROC3.2(hires)	3.44	2.55	6.38	5.94	9.60
MIROC3.2(medres)	4.69	4.00	7.46	5.70	9.17
INM-CM3.0	3.79	3.52	6.03	6.12	10.21
IPSL-CM4	3.97	3.33	6.59	6.43	11.44
ECHAM5/MPI-OM	5.08	4.68	6.52	5.33	10.95
ECHO-G	3.50	3.80	4.96	6.39	10.03
GISS-AOM	3.21	3.35	5.02	5.34	10.70
GISS-ER	3.46	4.84	6.70	4.79	8.19
MRI-CGCM2.3.2	2.63	3.48	5.67	6.35	10.79
CNRM-CM3	3.69	5.23	7.51	6.15	10.86
FGOALS-g1.0	3.30	3.34	6.48	6.43	11.29
GISS-EH	3.15	4.51	5.56	5.08	8.03
BCCR-BCM2.0	4.08	3.23	6.13	6.21	10.68
CCSM3	4.61	3.09	5.05	6.12	9.67
PCM	3.67	3.56	5.22	6.25	10.85
UKMO-HadCM3	2.66	3.03	5.94	6.21	10.13
UKMO-HadGEM1	3.85	3.86	5.78	5.95	9.53
Mean	3.65	3.75	5.98	5.96	10.39

Since climate simulations are not deterministic on interannual timescales, RMS has been determined based on the 5 year running means time series. Units: $Wm^{-2}a^{-1}$

Table 6 Correlations of observed annual all-sky SSR time series (5 year running means) with both simulated all-sky and clear-sky SSR time series, for the sites in Europe, Japan, southeast China, northwest China and India

Correlation	Europe		Japan		Southeast China		Northwest China		India	
	Obs/all sky mod	Obs/clear sky mod	Obs/all sky mod	Obs/clear sky mod	Obs/all sky mod	Obs/clear sky mod	Obs/all sky mod	Obs/clear sky mod	Obs/all sky mod	Obs/clear sky mod
CGCM3.1(T47)	0.07	0.56	−0.13	0.28	−0.25	0.16	0.64	0.83	0.03	0.50
CGCM3.1(T63)	0.18	0.80	0.13	0.49	−0.32	0.36	0.26	0.72	0.43	0.80
CSIRO-MK3.0	0.09	NaN	0.11	NaN	0.32	NaN	0.12	NaN	0.38	NaN
CSIRO-MK3.5	0.20	−0.03	−0.17	0.60	0.00	0.38	0.26	0.74	0.05	0.84
GFDL-CM2.0	0.51	0.81	0.44	0.63	0.13	0.52	0.55	0.90	0.61	0.78
GFDL-CM2.1	0.41	0.85	0.51	0.61	0.70	0.54	0.75	0.92	0.45	0.83
MIROC3.2(hires)	0.26	−0.40	0.54	0.69	0.26	0.42	0.67	0.52	0.66	0.79
MIROC3.2(medres)	−0.37	−0.46	0.47	0.65	0.57	0.40	0.86	0.66	0.54	0.76
INM-CM3.0	−0.31	0.41	0.06	0.47	−0.16	0.33	0.29	0.70	0.46	0.68
IPSL-CM4	0.09	0.54	0.16	0.49	0.36	0.36	0.16	0.90	−0.11	0.81
ECHAM5/MPI-OM	−0.54	0.16	0.34	0.52	0.42	0.46	0.89	0.92	−0.10	0.76
ECHO-G	0.24	0.57	0.25	0.64	0.14	0.60	0.56	0.90	0.83	0.77
GISS-AOM	0.41	NaN	−0.04	NaN	−0.10	NaN	0.77	NaN	0.33	NaN
GISS-ER	0.28	0.68	0.78	0.47	0.81	0.47	0.86	0.85	0.77	0.75
MRI-CGCM2.3.2	0.68	0.86	−0.01	0.66	−0.49	0.61	−0.13	0.87	0.62	0.64
CNRM-CM3	0.16	0.88	0.46	0.49	0.73	0.50	0.27	0.94	0.43	0.85
FGOALS-g1.0	0.35	0.64	−0.28	0.35	−0.37	0.18	0.12	0.80	−0.23	0.72
GISS-EH	0.45	0.78	0.75	0.79	0.53	0.58	0.87	0.90	0.64	0.72
BCCR-BCM2.0	−0.39	NaN	0.42	NaN	−0.04	NaN	0.29	NaN	0.31	NaN
CCSM3	−0.29	0.61	−0.10	0.67	0.02	0.49	0.07	0.57	0.36	0.74
PCM	0.24	NaN	−0.02	NaN	−0.64	NaN	0.18	NaN	0.70	NaN
UKMO-HadCM3	0.68	0.66	−0.07	0.66	0.67	0.57	0.36	0.62	0.40	0.73
UKMO-HadGEM1	0.02	−0.13	−0.19	0.62	0.19	0.52	0.17	0.63	0.76	0.78
Mean (19)	0.12	0.46	0.21	0.57	0.21	0.44	0.45	0.78	0.40	0.75

panel of Fig. 1 may not be overly realistic in the models, and are furthermore barely consistent.

4.2 Japan

Japan has a very good coverage with long-term SSR records. Similar to Europe, these records show a decline in SSR from the 1960s to the 1980s, and a partial recovery thereafter (e.g., Wild et al. 2005; Norris and Wild 2009; Ohmura 2009). This is reflected in the composite time series based on 25 of the most reliable Japanese sites as identified by Ohmura (2009), which shows a decline of SSR from the early 1960s to the 1980s of around 16 Wm^{-2}, and a subsequent increase of about 7 Wm^{-2} (Fig. 2, upper panel). This time series can also be reasonably approximated with a second order polynomial model. While this observation-based polynomial model shows a quadratic coefficient of 0.0295 $Wm^{-2}a^{-2}$, the range of the coefficients in the models is between −0.0111 $Wm^{-2}a^{-2}$ (UKMO-HadGEM1) and 0.0195 $Wm^{-2}a^{-2}$ (GISS-EH) (Table 3). 13 models show a concave behavior in the polynomial fit (6 of them significant), opposed to the qualitative shape of the observed time series, while only 10 models depict a convex behavior (4 of them significant) (Fig. 2, upper panel). Over the period 1961–1985, the observed linear decrease of SSR is −0.553 $Wm^{-2}a^{-1}$ (95% significant), while the models vary between −0.444 $Wm^{-2}a^{-1}$ (GISS-EH) and 0.25 $Wm^{-2}a^{-1}$(UKMO-HadGEM1), with a multi-model mean of −0.08 $Wm^{-2}a^{-1}$ (Table 4). 16 models show a decline in this period (8 significant), while 7 models show increases (4 significant). Over the 1985–2000 period, the observed linear increase in SSR is 0.577 $Wm^{-2}a^{-1}$ (significant), while the models vary between −0.551 $Wm^{-2}a^{-1}$ (MRI-CGCM2.3.2) and 0.366 $Wm^{-2}a^{-1}$ (CGCM3.1(T63)), with a multi-model mean of −0.08 $Wm^{-2}a^{-1}$. Only 9 models show an increase over this period (2 of them significant), whereas the majority of the models (14) show a continuing decline (8 significant) in contrast to observational evidence. Similarly to Europe, many models are not capable of reproducing the SSR variations qualitatively, and all of them underestimate them

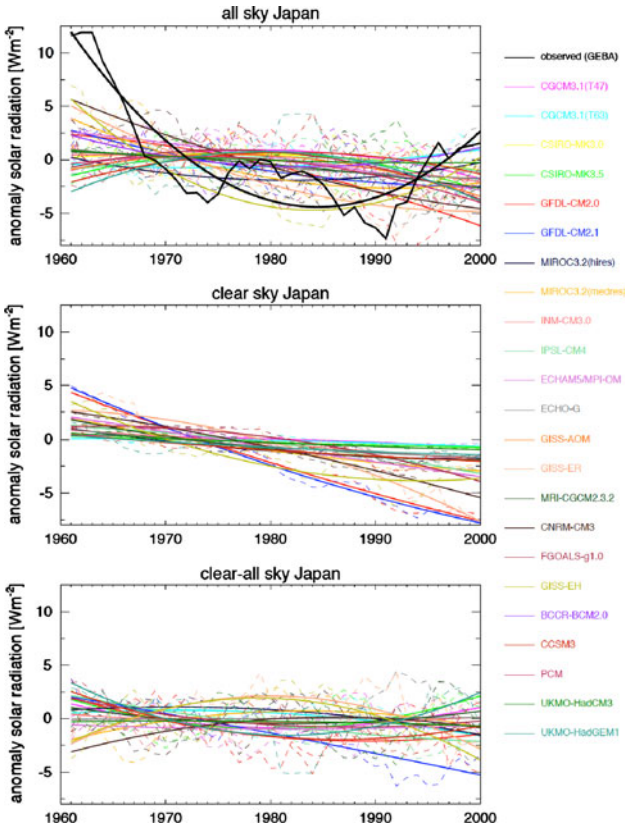

Fig. 2 As Fig. 1, but for 25 sites in Japan from 1961 to 2000

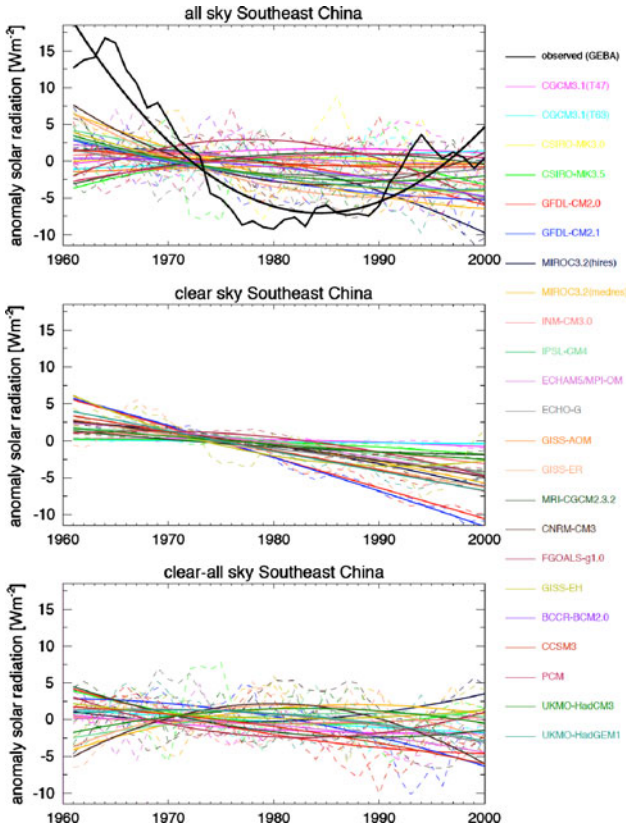

Fig. 3 As Fig. 1, but for six sites in Southeast China from 1961 to 2000

quantitatively. Again, for completeness, RMS statistics for the simulations over Japan are given in Table 5.

As in Europe, the evolution of clear-sky fluxes and cloud effects on SSR over Japan also largely varies (Fig. 2, middle and lower panel). A majority of the models simulate a convex shaped clear-sky time series as seen in the (all-sky) observations (12 out of 19). Again, the correlations of the smoothed time series are usually higher when the (all-sky) observations are correlated with the simulated clear-sky fluxes than with the simulated all-sky fluxes (Table 6). Here this is true for all but one of the models that provide both all-sky and clear-sky fluxes. Averaged over the 19 models, the correlation between the observed (all-sky) fluxes and the simulated clear-sky fluxes is 0.57, while no more than 0.21 between the observed (all-sky) fluxes and the more directly related simulated all-sky fluxes (Table 6). The cloud effects on SSR largely vary in the models over Japan (Fig. 2, lower panel), They disagree not only quantitatively, but also qualitatively, with 11 models showing a convex, and 8 models a concave evolution.

4.3 Southeast China

Numerous studies pointed to the strong decline of SSR between the 1950s and 1980s, and to a certain recovery during the 1990s in China (e.g., Wild et al. 2005; Shi et al. 2008; Norris and Wild 2009; Wild 2009a and references therein). This is also evident in the observed composite time series from six sites identified as most reliable by (Ohmura 2009) and shown in Fig. 3 (upper panel). Again a second order convex-shaped polynomial model describes the behavior of the observed time series best. This composite time series shows the strongest dimming/brightening of all regions considered, with a quadratic coefficient of 0.0476 $Wm^{-2}a^{-2}$ in the polynomial fit (Table 3). The observed decrease of SSR until the mid 1980s was as much as 25 Wm^{-2}, the subsequent increase nearly 12 Wm^{-2}. 11 models qualitatively reproduce this overall behavior of a dimming with subsequent brightening and a convex shaped polynomial (Fig. 3 upper panel, Table 3). The other half of the models again does not even qualitatively reproduce this overall behavior, showing a concave shaped second order polynomial approximation. The quadratic coefficient in the models as shown in Table 3 ranges from -0.0177 $Wm^{-2}a^{-2}$ (FGOALS-g1.0) to 0.0190 $Wm^{-2}a^{-2}$ (CNRM-CM3). None of the models thus reproduces the strong recurvature as indicated in the observed composite record. When separated into the dimming and brightening periods, the observed linear decrease from 1961 to 1985 is

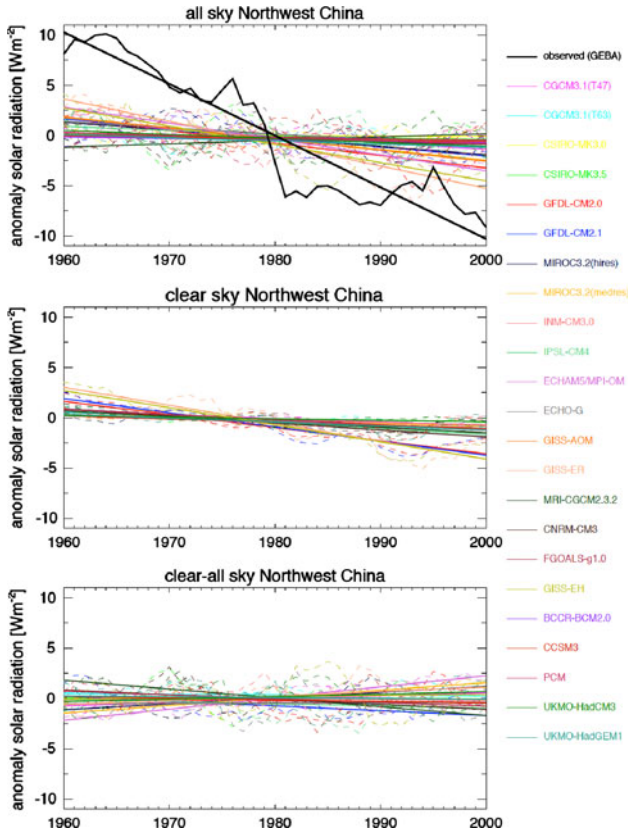

Fig. 4 As Fig. 1, but for seven sites in Northwest China from 1960 to 2000

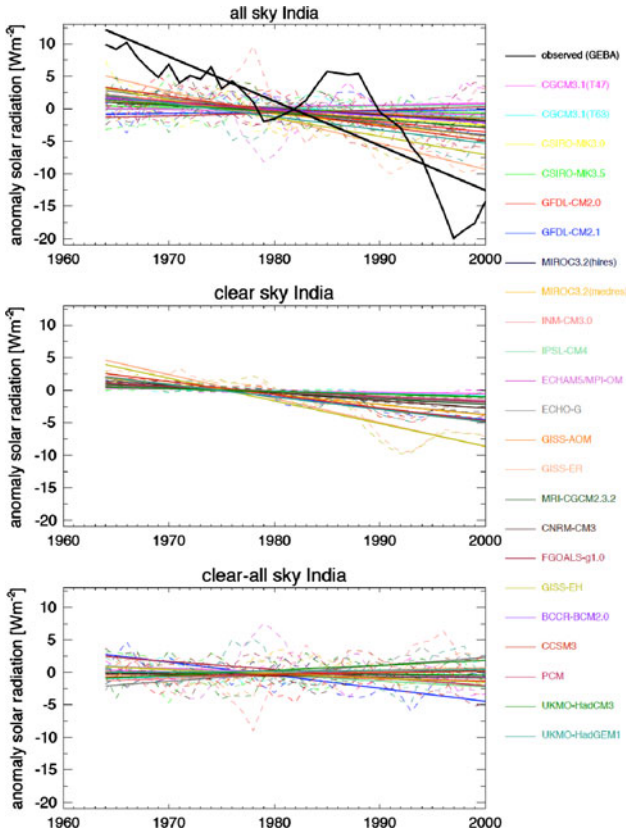

Fig. 5 As Fig. 1, but for four sites in India from 1964 to 2000

1.230 $Wm^{-2}a^{-1}$ (95% significant), while the increase of SSR between 1985 and 2000 is 0.682 $Wm^{-2}a^{-1}$ (95% significant). The linear trends in the models vary from −0.475 (CNRM-CM3) to 0.211 $Wm^{-2}a^{-1}$ (PCM) in the 1961–1985 period, with a multi-model mean of -0.131 $Wm^{-2}a^{-1}$. 16 models show a linear decrease during this period (9 significant) in qualitative agreement with the observed records, but the multi-model mean decrease is an order of magnitude smaller than the decrease seen in the observations. In the second period from 1985 to 2000 the models vary from −0.872 (MIROC3.2(hires)) to 0.523 $Wm^{-2}a^{-1}$ (CNRM-CM3), with a multi-model mean of -0.186 $Wm^{-2}a^{-1}$. In contrast to the observations, 15 models show a decrease (8 significant), while only 8 models show an increase (2 of them significant). The majority of the models therefore neither reproduces the strong downward SSR trends up the 1980s nor its partial recovery in the 1990s in Southeast China.

The evolution of clear-sky fluxes and particularly cloud effects over South East China also shows considerable differences (Fig. 3, middle and lower panel). Correlations of the smoothed time series are higher here in 14 out of 19 models when the (all-sky) observations are correlated with the simulated clear-sky fluxes than with the simulated all-sky fluxes (Table 6). Averaged over the 19 models, the correlation between the (all-sky) observations and the simulated clear-sky fluxes is 0.44, while no more than 0.21 between the (all-sky) observations and the more directly related simulated all-sky fluxes (Table 6).

Also, as in Europe and Japan, cloud effects on SSR do not show a great deal of consistency, with nine of the models showing a convex evolution, and ten of the models a concave evolution.

4.4 Northwest China

In contrast to Southeast China, the observed composite time series, based on seven sites in Northwest China, does not show a strong recovery in the 1990s. Therefore the continuous decrease over the entire period can be reasonably approximated with a first order linear polynomial. For compatibility, we use also first order polynomials to describe the model-calculated time series, even though some of the model time series would have significant coefficients when approximated with second order polynomials.

The observed decline of SSR over the period 1960–2000 is on the order of 20 Wm^{-2}, or −0.5146 $Wm^{-2}a^{-1}$ (95% significant). The linear trends over the same period in the

models vary from -0.2224 $Wm^{-2}a^{-1}$ (GISS-ER) to 0.0335 $Wm^{-2}a^{-1}$ (MRI-CGCM2.3.2), with a multi-model mean of -0.0627 $Wm^{-2}a^{-1}$ (Table 3, Fig. 4 upper panel). 22 models reproduce the negative trend in SSR qualitatively (10 significant), only the MRI-CGCM2.3.2 shows a positive trend, which is not significant. However, all these models show a much smaller decrease than the observed time series, with the multi-model mean decrease being almost an order of magnitude smaller than the observed decrease.

The observations indicate further a substantially smaller decline during the 1985–2000 period (decline -0.208 $Wm^{-2}a^{-1}$) than during the 1960–1985 period (decline -0.649 $Wm^{-2}a^{-1}$) (Table 4). This is qualitatively only reproduced in 5 out of 23 models (Table 4). RMS statistics for the simulations in both Chinese regions are found again in Table 5.

All models show a decrease in the clear sky fluxes over the period considered (Fig. 4, middle panel), but of different magnitude, covering a range between -0.02 $Wm^{-2}a^{-1}$ and -0.18 $Wm^{-2}a^{-1}$. The sign of the tendencies in the cloud effect is much less consistent (Fig. 4, lower panel), with 8 models showing an overall increase in the cloud effect, while 11 models simulate a decrease. Not surprisingly therefore, also in Northwest China, correlations of the smoothed time series are higher, when the (all-sky) observations are correlated with the simulated clear-sky fluxes rather than with the simulated all-sky fluxes (Table 6), this time in 16 out of 19 models. Averaged over the 19 models, the correlation between the observations and the simulated clear-sky fluxes is as high as 0.78, while 0.45 between the observations and the more directly related simulated all-sky fluxes (Table 6).

4.5 India

Similarly to the region in Northwest China, the observed radiation records in India show a continuous decrease in SSR from 1964 to 2000 with no substantial recovery in the more recent period (Wild et al. 2005; Ramanathan et al. 2005; Kumari et al. 2007; Ohmura 2009). This is illustrated in Fig. 5 (upper panel), where a composite time series of the four most complete observational records is shown. A linear model has therefore again been used to approximate this time series. The observed decline of SSR over the entire 1960s to 2000 period is very similar to the one in Northwest China and is nearly 25 Wm^{-2}, corresponding to a linear trend of -0.686 $Wm^{-2}a^{-1}$ (95% significant) (Table 3, Fig. 5 upper panel). The linear trends in the models range from -0.400 $Wm^{-2}a^{-1}$ (GISS-ER) to 0.045 $Wm^{-2}a^{-1}$ (FGOALS-g1.0), with a multi-model mean of -0.116 $Wm^{-2}a^{-1}$. 19 models have a negative trend in qualitative agreement with the observational evidence (16 of them significant), while 4 models show a positive trend opposed to the observations (none of them being significant). However, as in Northwest China, even though most models qualitatively reproduce the overall decline over the 1964–2000 period, the decline is much smaller than suggested by the observations.

Under clear-sky conditions, all 19 models that provide clear-sky fluxes show an overall decrease (statistically significant at the 95% level), but again of largely varying magnitude (between -0.02 $Wm^{-2}a^{-1}$ to -0.37 $Wm^{-2}a^{-1}$.) As in all other regions considered before, also in India correlations of the smoothed time series are higher, when the all-sky observations are correlated with the simulated clear-sky fluxes than with the more comparable simulated all-sky fluxes (Table 6). This is found in as many as 17 out of 19 models. Averaged over the 19 models, the correlation between the all-sky observations and the simulated clear-sky fluxes is 0.75, while 0.40 between the all-sky observations and the more directly related simulated all-sky fluxes (Table 6). The largely variable and highly inconsistent simulation of cloud effects (Fig. 5, lower panel) contributes to the poorer correlation of the all-sky fluxes with the observations compared to the clear-sky fluxes. Specifically, the cloud effect on SSR declines in 10 and increases in 9 of the models over the period under consideration.

4.6 Dimming/brightening in ERA 40

In addition to the above models, we also investigated the SSR evolution as determined in the reanalysis carried out by the European Center for Medium Range Weather Forecasting over the periods 1958–2002 (ERA-40, Uppala et al. 2005). Compared to GCMs, reanalyses have the advantage that they assimilate the comprehensive weather data from the global observing system (GOS) every 6 h into their atmospheric models. Further, the evolution of the sea surface temperature in reanalyses is prescribed from observations in contrast to the GCMs considered in this study, which calculate them within their coupled atmosphere–ocean modeling frameworks. The physical and dynamical state of the atmosphere in reanalyses is therefore strongly constrained by observations, in contrast to the pure GCMs discussed before. Therefore it might be expected, that the temporal evolution of the atmospheric state is more deterministic and better reproduced in reanalyses than in the unconstrained GCMs above. Thus it is also interesting to see how the evolution of SSR is reproduced in a reanalysis with an extended integration period that covers both dimming and brightening phases, such as in ERA-40.

The observed composite SSR time series based on the nine sites in Europe (as used in Sect. 4.1) is now compared with the corresponding time series from ERA-40 in Fig. 6a.

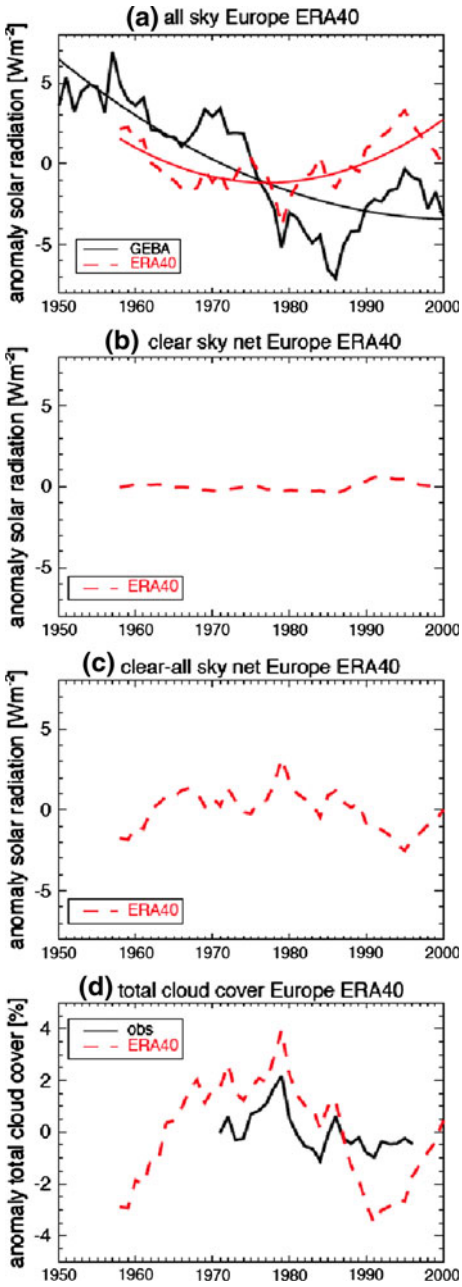

Fig. 6 Annual observed surface solar radiation and cloud anomalies from 1950 to 2000 as composite of 9 sites in Europe (*solid curves*), and corresponding simulation by ERA-40 (*red dashed curve*). **a** all-sky fluxes, **b** clear sky fluxes, **c** surface cloud effect (defined as difference of clear and all-sky fluxes) **d** cloud amount. Radiation observations from GEBA (only available for all-sky conditions), collocated synoptic cloud observations from CDIAC, available for the period 1971–1996 (Warren et al. 2007). Time series are shown as 5-year running means. Also added are second order polynomial fits for the all-sky time series

The ERA-40 time series (red dashed line) shows an SSR dimming and subsequent brightening, however with an earlier turning point and a more pronounced brightening than indicated by the observations. A further analysis of the SSR evolution under clear-sky and the cloud effects (Figs. 6b, c) reveals that the SSR dimming and brightening in ERA-40 is predominantly induced by changes in the cloud effects (Fig. 6c), while changes in clear- sky SSR are negligible (Fig. 6b). This is in contrast to recent evidence that aerosol effects are the main cause of dimming/brightening in Europe (Norris and Wild 2007; Ruckstuhl et al. 2008). Note, however, that ERA-40 does not include time-dependent aerosol burdens, but rather a time invariant aerosol climatology (Tanre et al. 1984). The ERA-simulated cloud amount variations at the same nine sites is further compared with a composite time series of collocated synoptic (surface-based) cloud observations, provided by the Carbon Dioxide Information Analysis Center (CDIAC) of the United States Department of Energy, available for the period 1971–1996 (Warren et al. 2007). A comparison in Fig. 6d suggests that the strong ERA-40-simulated decline in cloud amount after 1980, which is at the origin of the strong brightening in the ERA-40, is not found to the same extent in the observations.

Similarly to Europe, a strong brightening is found in the ERA-40-determined SSR also at the Japanese sites (Fig. 7a), caused by a strong decline of the cloud effect (Fig. 7c), while again the clear-sky SSR shows hardly any change due to the time-invariant aerosol climatology, in contrast to observational evidence (Norris and Wild 2009). A comparison of the collocated synoptic cloud observations with ERA-40-estimated cloud amount changes at these sites suggests that the strong decline in cloud amount estimated in ERA-40 between the mid-1970s and 1990 is not in accordance with observational evidence. This suggests that, as in Europe, the brightening in Japan in ERA-40 might be due to the wrong reason (decline in clouds rather than aerosol as suggested in observational studies).

Observed dimming and brightening at the composite of six sites in southeast China is not captured at all by the ERA-40 (Fig. 8a). In this region an extended literature exists that demonstrates that the strong dimming and consecutive slight recovery in the 1990s is dominated by modulation of SSR under clear-sky conditions due to changes in aerosol burden and composition (e.g., Liu et al. 2004; Qian et al. 2007; Norris and Wild 2009). Since the ERA-40 does not consider any of these effects (Fig. 8b), it is not surprising that the observed strong decadal changes are completely absent. The same is also true for the seven sites in northwest China, where the strong dimming is not captured in ERA-40 (Fig. 9a), since SSR does not show any noticeable changes under cloud-free conditions (Fig. 9b).

Similarly to China, also in India the continuous strong dimming is dominated by reductions of solar radiation under cloud-free conditions, due to the strong increase in air pollution and associated aerosol burden, such as the

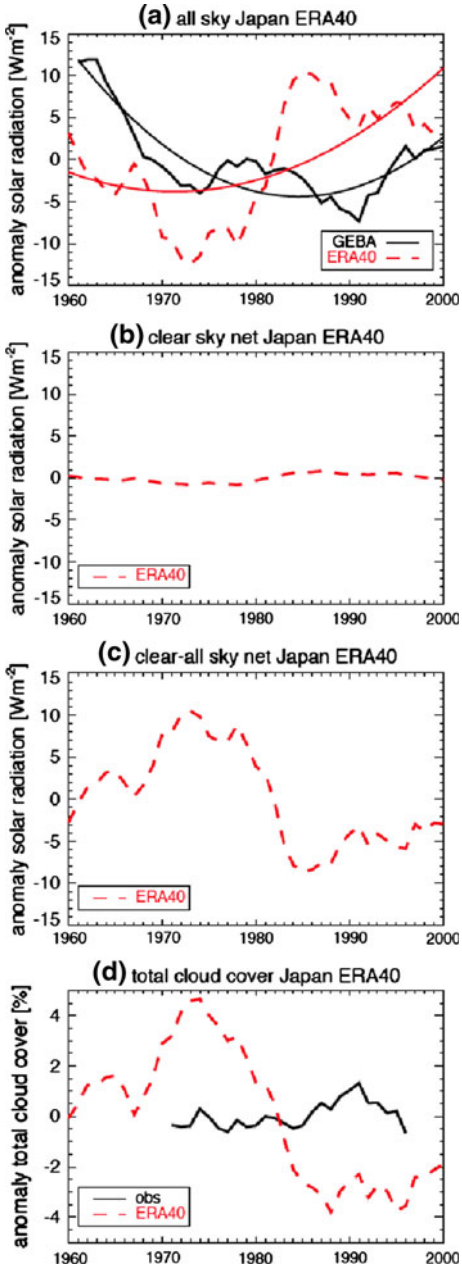

Fig. 7 As Fig. 6, but for 25 sites in Japan from 1961 to 2000

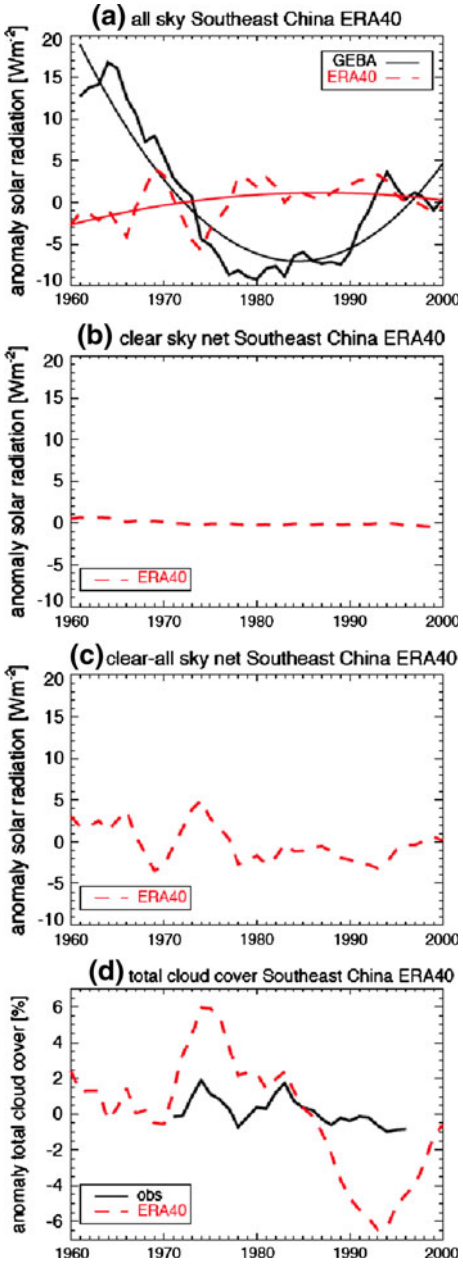

Fig. 8 As Fig. 6, but for six sites in Southeast China from 1961 to 2000

Asian Brown Cloud (ABC, Ramanathan et al. 2005). None of this is seen in ERA-40 (Fig. 10b), and since cloud cover is decreasing at the Indian sites, in reasonable agreement with observations (Fig. 10d), ERA-40 simulates an overall brightening from 1960 to 2000 at the sites in India, opposed to observational evidence (Fig. 10a). The failure of ERA-40 to represent the main characteristics of the decadal variations of SSR, despite substantial observational constraints on the dynamical and physical structure of the atmosphere, points to the importance of aerosol changes in this context, which are not included in ERA-40.

5 Discussion and conclusion

The analyses showed that the substantial decadal variations in SSR detected in long-term observational records in various regions of the world are not similarly reproduced in currently accessible climate model simulations and in a long-term reanalysis (ERA40). Many of the models do not reproduce the strong observed tendencies in a qualitative way, and all of the models show much smaller amplitudes in SSR variations than indicated by the observations. Of course to some extent biases can be introduced by

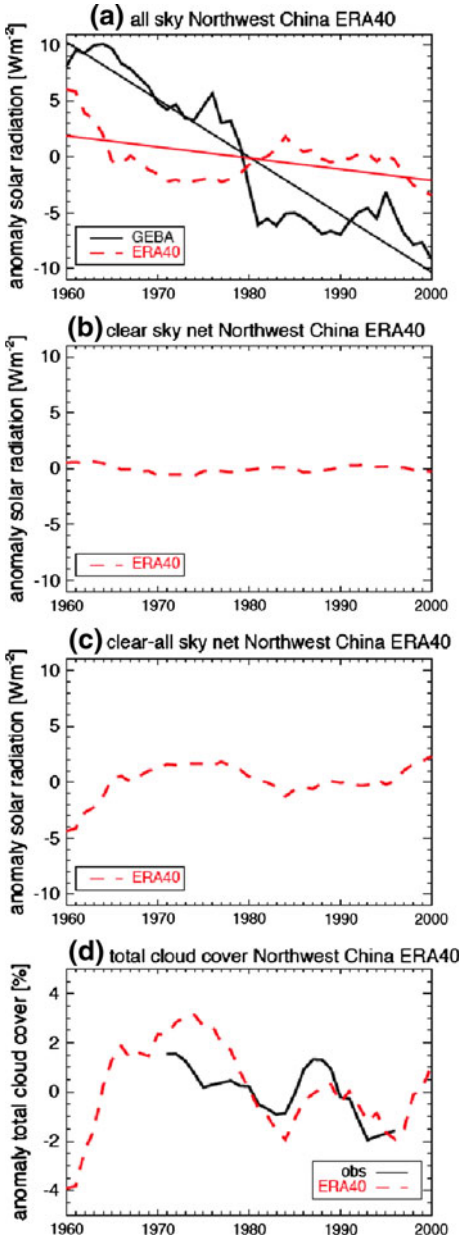

Fig. 9 As Fig. 6, but for seven sites in Northwest China from 1960 to 2000

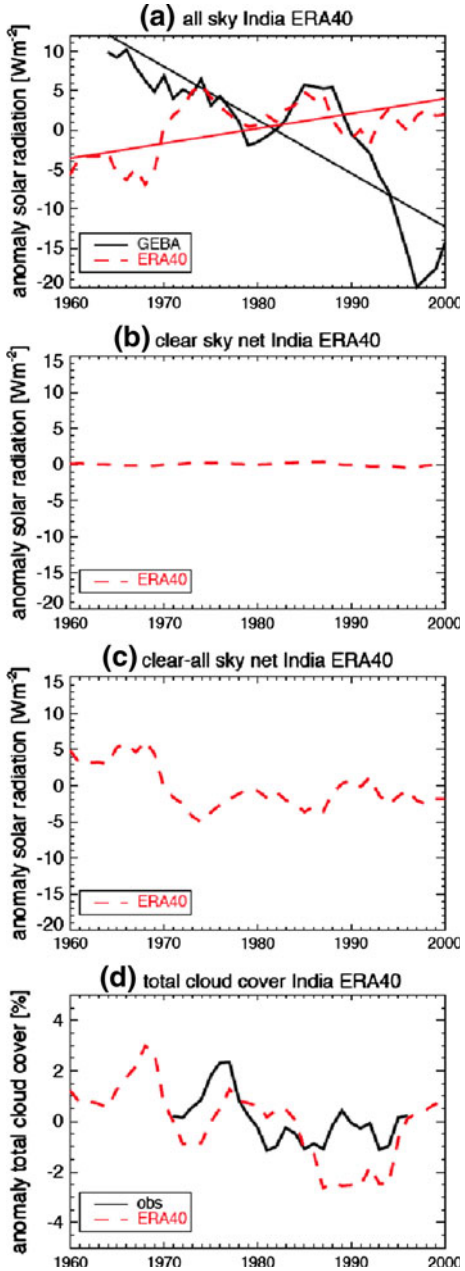

Fig. 10 As Fig. 6, but for four sites in India from 1964 to 2000

comparing model fields with point observations (but see discussion in Xi et al. 2010, Kennedy et al. 2010). Observation sites may be influenced by local air pollution particularly in heavily urbanized areas (Alpert et al. 2005). This effect so far is neither well established nor quantified. We minimized this potential influence in that we only considered composites of GCM grid-points nearest to the station location, and did not attempt to extrapolate to large scale or regional averages. Also, the rural observation sites (e.g., Hohenpeissenberg, Toravere; Russak 2009) used in this study show similar dimming and brightening amplitudes as other more urbanized sites.

Surprisingly, the (all-sky) observations often correlate better with the model-simulated clear-sky fluxes than with the more appropriately comparable all-sky fluxes on decadal time scales. This suggests that the consideration of variations of cloud effects in the models rather deteriorates than improves the simulation of decadal variations in SSR, and points to substantial problems still inherent in the adequate simulation of temporally varying cloud characteristics. However, even though the simulated clear-sky SSR variations agree better with the observed (all-sky) fluxes in their qualitative evolution, quantitatively they are too small to explain a significant fraction of the observed

(all-sky) variations (cf. middle and upper panels in Figs. 1, 2, 3, 4, 5). Possible reasons are the inaccuracies or entire lack of variation in the aerosol fields used in the models. Uncertainties and inconsistencies in aerosol emission and burdens in different IPCC-AR4 models over Europe were identified in Ruckstuhl and Norris (2009). It was argued therein that the poor agreement between modeled and observed clear-sky ''dimming'' and ''brightening'' over Europe is due to incorrect aerosol emission histories. In most models, aerosols are prescribed as atmospheric burdens rather than interactively calculated from prescribed emissions, which would allow for more degrees of freedom. Also, most of the models only consider sulfate aerosol and do not include additional aerosol types, such as black carbon (see Table 1). This further reduces the degrees of freedom of the aerosol representation in the models and its effects on SSR. Amongst the models that generally perform better compared to the observations are some of those that include in addition black carbon (GISS-EH, GISS-ER, GFDL-CM2.0/2.1, MIROC3.2, UKMO-HADGEM1, CCSM3). This is seen particularly in areas with strong pollution such as in India, where these models simulate the strongest decline in better agreement with observations (strongest SSR declines in GISS-EH, GISS-ER, CCSM3, UKMO-HADGEM1, c.f. Table 3).

On the other hand, if aerosol characteristics are only included on a climatological mean basis with no temporal resolution, decadal SSR variations cannot be reproduced adequately even when other physical properties of the atmosphere are optimally constraint by observations as done in the ERA-40 reanalysis. ERA-40 misses major decadal changes in SSR particularly in heavily polluted regions, such as the well-established long-term dimming in China and India. This again points to the importance of an adequate representation of time varying aerosol effects for a realistic simulation of decadal variations in SSR and associated dimming and brightening.

The inability of climate models to simulate the full extent of decadal-scale variability is not just seen in SSR as documented in the present study, but also in other simulated climate elements such as the tropical top of atmosphere radiation budget (Wielicki et al. 2002), tropical precipitation (Allan and Soden 2007), the hydrological cycle in general (Wild and Liepert 2010), soil moisture (Li et al. 2007) and surface temperature/diurnal temperature range (Wild 2009b). Of course these elements may not be entirely independent, and misrepresentation of decadal variations in one of these, such as the SSR discussed here, may strongly impact the simulation of others. Further work is necessary to disentangle to what extent these underestimated decadal variations are due to an underestimation of forced or unforced climate variability.

The inability of current GCMs to reproduce observed decadal scale variations does not imply that climate change scenarios (which typically target at more extended timescales) are biased. On these longer, multi-decadal to centennial timescales comparison with observations show good agreement where feasible, despite suppressed decadal variations (e.g. IPCC 2007; Wild 2009b). However, the shortcomings discussed here may have implications for shorter-term climate projections up to a few decades ahead where these strong decadal variations may dominate.

Acknowledgments This study is supported by the National Centre for Competence in Climate Research (NCCR Climate) of the Swiss National Science Foundation. We would like to thank Prof. Christoph Schaer for the continuous support of our work. We acknowledge the international modeling groups for providing their data for analysis, the Program for Climate Model Diagnosis and Intercomparison (PCMDI) for collecting and archiving the model data, the JSC/CLIVAR Working Group on Coupled Modelling (WGCM) and their Coupled Model Intercomparison Project (CMIP) and Climate Simulation Panel for organizing the model data analysis activity, and the IPCC WG1 TSU for technical support. The IPCC Data Archive at Lawrence Livermore National Laboratory is supported by the Office of Science, U.S. Department of Energy. Doris Folini is highly acknowledged for her support of this study. We highly appreciate the constructive comments of two anonymous reviewers. This paper contributes to the efforts of the working group "Global Energy Balance" of the International Radiation Commission (IRC).

References

Allan RP, Soden BJ (2007) Large discrepancy between observed and simulated precipitation trends in the ascending and descending branches of the tropical circulation. Geophys Res Lett 34(18):L18705. doi:10.1029/2007gl031460

Alpert P, Kishcha P, Kaufman YJ, Schwarzbard R (2005) Global dimming or local dimming? Effect of urbanization on sunlight availability. Geophys Res Lett 32(17):L17802. doi:10.1029/2005gl023320

Chiacchio M, Wild M (2010) Influence of nao and clouds on long-term seasonal variations of surface solar radiation in europe. J Geophys Res Atmospheres 115:D00d22. doi:10.1029/2009jd012182

Gilgen H, Ohmura A (1999) The global energy balance archive. Bull Am Meteorol Soc 80(5):831–850

Gilgen H, Wild M, Ohmura A (1998) Means and trends of shortwave irradiance at the surface estimated from global energy balance archive data. J Clim 11(8):2042–2061

Gilgen H, Roesch A, Wild M, Ohmura A (2009) Decadal changes in shortwave irradiance at the surface in the period from 1960 to 2000 estimated from global energy balance archive data. J Geophys Res Atmospheres 114:D00d08. doi:10.1029/2008jd011383

IPCC (2007) Climate change 2007: the physical science basis. Contribution of working group I to the fourth assessment report of the intergovernmental panel on climate change. Cambridge, United Kingdom and New York, NY, USA

Kennedy A, Dong X, Xi B, Minnis P, Del Genio A, Wolf A, Khaiver M (2010) Evaluation of the NASA GISS single column model simulated clouds using combined surface and satellite observations. J Climate 23:5175–5192. doi:10.1175/2010JCLI3353.1

Kumari BP, Londhe AL, Daniel S, Jadhav DB (2007) Observational evidence of solar dimming: offsetting surface warming over india. Geophys Res Lett 34(21):L21810. doi:10.1029/2007gl031133

Li HB, Robock A, Wild M (2007) Evaluation of intergovernmental panel on climate change fourth assessment soil moisture simulations for the second half of the twentieth century. J Geophys Res Atmospheres 112(D6):D06106. doi:10.1029/2006jd007455

Liepert BG (1990) Observed reductions of surface solar radiation at sites in the united states and worldwide from 1961 to 1990. Geophys Res Lett 29(10):1421. doi:10.1029/2002gl014910

Liu BH, Xu M, Henderson M, Qi Y, Li YQ (2004) Taking china's temperature: daily range, warming trends, and regional variations, 1955–2000. J Clim 17(22):4453–4462

Makowski K, Jaeger EB, Chiacchio M, Wild M, Ewen T, Ohmura A (2009) On the relationship between diurnal temperature range and surface solar radiation in Europe. J Geophys Res Atmospheres 114:D00d07. doi:10.1029/2008jd011104

Norris JR, Wild M (2007) Trends in aerosol radiative effects over europe inferred from observed cloud cover, solar "Dimming" And solar "Brightening". J Geophys Res Atmospheres 112(D8):D08214. doi:10.1029/2006jd007794

Norris JR, Wild M (2009) Trends in aerosol radiative effects over china and japan inferred from observed cloud cover, solar "Dimming", and solar "Brightening''. J Geophys Res Atmospheres 114:D00d15. doi:10.1029/2008jd011378

Ohmura A (2009) Observed decadal variations in surface solar radiation and their causes. J Geophys Res Atmospheres 114:D00d05. doi:10.1029/2008jd011290

Ohmura A, Gilgen H (1993) Reevaluation of the global energy balance. In: McBean GA, Hantel M (eds) Interactions between global climate subsystems - the legacy of hann, vol 75. Geophysical monograph series. Amer Geophysical Union, Washington, pp 93–110

Ohmura A, Lang H (1989) Secular variations of global radiation in europe. Paper presented at the IRS '88: current problems in atmospheric radiation, Lille, France

Ohmura A, Gilgen H, Wild M (1989) Global energy balance archive geba, world climate program–water project a7. *Zuercher Geografische Schriften*, vol 34. Zuerich

Qian Y, Wang WG, Leung LR, Kaiser DP (2007) Variability of solar radiation under cloud-free skies in china: the role of aerosols. Geophys Res Lett 34(12):L12804. doi:10.1029/2006gl028800

Ramanathan V, Chung C, Kim D, Bettge T, Buja L, Kiehl JT, Washington WM, Fu Q, Sikka DR, Wild M (2005) Atmospheric brown clouds: impacts on south Asian climate and hydrological cycle. Proc Natl Acad Sci USA 102(15):5326–5333. doi:10.1073/pnas.0500656102

Romanou A, Liepert B, Schmidt GA, Rossow WB, Ruedy RA, Zhang Y (2007) 20th century changes in surface solar irradiance in simulations and observations. Geophys Res Lett 34(5):L05713. doi:10.1029/2006gl028356

Ruckstuhl C, Norris JR (2009) How do aerosol histories affect solar "Dimming" And "Brightening" Over europe? Ipcc-ar4 models versus observations. J Geophys Res Atmospheres 114:D00d04. doi:10.1029/2008jd011066

Ruckstuhl C, Philipona R, Behrens K, Coen MC, Durr B, Heimo A, Matzler C, Nyeki S, Ohmura A, Vuilleumier L, Weller M, Wehrli C, Zelenka A (2008) Aerosol and cloud effects on solar brightening and the recent rapid warming. Geophys Res Lett 35(12):L12708. doi:10.1029/2008gl034228

Russak V (2009) Changes in solar radiation and their influence on temperature trend in estonia (1955–2007). J Geophys Res Atmospheres 114:D00d01. doi:10.1029/2008jd010613

Shi GY, Hayasaka T, Ohmura A, Chen ZH, Wang B, Zhao JQ, Che HZ, Xu L (2008) Data quality assessment and the long-term trend of ground solar radiation in china. J Appl Meteorol Climatol 47(4):1006–1016. doi:10.1175/2007jamc1493.1

Stanhill G, Cohen S (2001) Global dimming: a review of the evidence for a widespread and significant reduction in global radiation with discussion of its probable causes and possible agricultural consequences. Agric For Meteorol 107(4):255–278

Tanre D, Geleyn J-F, Slingo JM (1984) First results of the introduction of an advanced aerosol-radiation interaction in the ECMWF low resolution global model. In: Gerber HE, Deepak A (eds) Aerosols and their climatic effects. Deepak, Hampton, pp 133–177

Uppala SM, Kallberg PW, Simmons AJ, Andrae U, Bechtold VD, Fiorino M, Gibson JK, Haseler J, Hernandez A, Kelly GA, Li X, Onogi K, Saarinen S, Sokka N, Allan RP, Andersson E, Arpe K, Balmaseda MA, Beljaars ACM, Van De Berg L, Bidlot J, Bormann N, Caires S, Chevallier F, Dethof A, Dragosavac M, Fisher M, Fuentes M, Hagemann S, Holm E, Hoskins BJ, Isaksen L, Janssen PAEM, Jenne R, McNally AP, Mahfouf JF, Morcrette JJ, Rayner NA, Saunders RW, Simon P, Sterl A, Trenberth KE, Untch A, Vasiljevic D, Viterbo P, Woollen J (2005) The era-40 re-analysis. Q J Roy Meteorol Soc 131(612):2961–3012. doi:10.1256/Qj.04.176

Warren SG, Eastman RM, Hahn CJ (2007) A survey of changes in cloud cover and cloud types over land from surface observations, 1971–96. J Clim 20(4):717–738. doi:10.1175/Jcli4031.1

Wielicki BA, Wong TM, Allan RP, Slingo A, Kiehl JT, Soden BJ, Gordon CT, Miller AJ, Yang SK, Randall DA, Robertson F, Susskind J, Jacobowitz H (2002) Evidence for large decadal variability in the tropical mean radiative energy budget. Science 295(5556):841–844

Wild M (2005) Solar radiation budgets in atmospheric model intercomparisons from a surface perspective. Geophys Res Lett 32(7):L07704. doi:10.1029/2005gl022421

Wild M (2008) Short-wave and long-wave surface radiation budgets in gcms: a review based on the ipcc-ar4/cmip3 models. Tellus A 60(5):932–945. doi:10.1111/J.1600-0870.2008.00342.X

Wild M (2009a) Global dimming and brightening: a review. J Geophys Res Atmospheres 114:D00d16. doi:10.1029/2008jd011470

Wild M (2009b) How well do ipcc-ar4/cmip3 climate models simulate global dimming/brightening and twentieth-century daytime and nighttime warming? J Geophys Res Atmospheres 114:D00d11. doi:10.1029/2008jd011372

Wild M, Liepert B (2010) The earth radiation balance as driver of the global hydrological cycle. Environ Res Lett 5(2):Artn 025003. doi:10.1088/1748-9326/5/2/025003

Wild M, Gilgen H, Roesch A, Ohmura A, Long CN, Dutton EG, Forgan B, Kallis A, Russak V, Tsvetkov A (2005) From dimming to brightening: decadal changes in solar radiation at earth's surface. Science 308(5723):847–850. doi:10.1126/science.1103215

Wild M, Long CN, Ohmura A (2006) Evaluation of clear-sky solar fluxes in gcms participating in AMIP and IPCC-AR4 from a surface perspective. J Geophys Res Atmospheres 111(D1):D01104. doi:10.1029/2005jd006118

Wild M, Truessel B, Ohmura A, Long CN, Konig-Langlo G, Dutton EG, Tsvetkov A (2009) Global dimming and brightening: an update beyond 2000. J Geophys Res Atmospheres 114:D00d13. doi:10.1029/2008jd011382

Xi B, Dong X, Minnis P, Khaiyer MM (2010) A 10-year climatology of cloud cover and vertical distribution derived from both surface and GOES observations over the DOE ARM SGP Site. J Geophys Res Atmospheres 115:D12124. doi:10.1029/2009JD012800